Chinese Journal of Natural Medicines

Saponins from *Aralia taibaiensis* protect against brain ischemia/reperfusion injuries by regulating the apelin/AMPK pathway

Zhengrong Li, Yuwen Liu, Kedi Liu, Xingru Tao, Naping Hu, Wangting Li, Jialin Duan

Citation: Zhengrong Li, Yuwen Liu, Kedi Liu, Xingru Tao, Naping Hu, Wangting Li, Jialin Duan, Saponins from *Aralia taibaiensis* protect against brain ischemia/reperfusion injuries by regulating the apelin/AMPK pathway, Chinese Journal of Natural Medicines, 2025, 23(3), 299−310. doi: 10.1016/S1875−5364(25)60841−7.

View online: https://doi.org/10.1016/S1875−5364(25)60841−7

Chinese Journal of Natural Medicines 23 (2025) 299-310

Contents lists available at ScienceDirect

Chinese Journal of Natural Medicines

journal homepage: www.cjnmcpu.com/

Original article

Saponins from *Aralia taibaiensis* protect against brain ischemia/reperfusion injuries by regulating the apelin/AMPK pathway

Zhengrong Li[a,Δ], Yuwen Liu[a,Δ], Kedi Liu[b,Δ], Xingru Tao[c], Naping Hu[d], Wangting Li[c], Jialin Duan[a,e,*]

[a] *Xi'an Key Laboratory of Stem Cell and Regenerative Medicine, Institute of Medical Research, Northwestern Polytechnical University, Xi'an 710072, China*
[b] *TANK Medicinal Biology Institute of Xi'an, Xi'an 710065, China*
[c] *Department of Pharmacy, Xijing Hospital, Fourth Military Medical University, Xi'an 710032, China*
[d] *Department of Pharmacy, General Hospital of Xinjiang Production and Construction Corps, Urumqi 830092, China*
[e] *Shanghai Minhang Collaborative Innovation Center of Northwestern Polytechnical University, Shanghai 201108, China*

ARTICLE INFO

Article history:
Received 13 December 2023
Revised 7 April 2024
Accepted 10 May 2024
Available online 20 April 2025

Keywords:
Aralia taibaiensis
Apelin/apelin receptor
Stroke
P38 MAPK/ATF4
HIF-1a

ABSTRACT

Aralia taibaiensi, widely distributed in western China, particularly in the Qinba Mountains, has been utilized as a folk medicine for treating diabetes, gastropathy, rheumatism, and cardiovascular diseases. Saponins from *A. taibaiensis* (sAT) have demonstrated protective effects against oxidative stress and mitochondrial dysfunction induced by ischemia/reperfusion (I/R). However, the underlying mechanisms remain unclear. *In vivo*, middle cerebral artery occlusion/reperfusion (MCAO/R) induced inflammatory infiltration, neuronal injury, cell apoptosis, mitochondrial dysfunction, and oxidative stress in the ischaemic penumbra, which were effectively mitigated by sAT. sAT increased the mRNA and protein expression levels of apelin and its receptor apelin/apelin receptors (ARs) both *in vivo* and *in vitro*. (Ala13)-Apelin-13 (F13A) and small interfering RNA (siRNA) abolished the regulatory effects of sAT on neuroprotection mediated by adenosine 5'-monophosphate (AMP)-activated protein kinase (AMPK)/protein kinase B (Akt). Furthermore, sAT induced apelin/AR expression by simultaneously inhibiting P38 mitogen-activated protein kinase (P38 MAPK)/activating transcription factor 4 (ATF4) and upregulating hypoxia-inducible factor-1α (HIF-1α). Our findings indicate that sAT regulates apelin/AR/AMPK by inhibiting P38 MAPK/ATF4 and upregulating HIF-1a, thereby suppressing oxidative stress and mitochondrial dysfunction.

1. Introduction

The genus *Aralia* is widely distributed and traditionally used in China, Japan, Korea, and the Americas for medicinal purposes. The first recorded use of *Aralia* species in medicine dates back to the Tang Dynasty (A.D. 652) in China, as documented in the "Qian Jin Fang", and is also mentioned in the "Materia Medica of Southern Yunnan", Ming Dynasty, (A.D. 1436) and "Compendium of Materia Medica", Ming Dynasty, (A.D. 1578). These historical texts indicate its use in treating rheumatism, lumbosacral pain, and swelling and pain associated with sprains and fractures [1]. Currently, several pharmaceutical formulations containing *Aralia* have been developed and marketed in China. Multiple clinical and preclinical studies have demonstrated significant efficacy in treating metabolic diseases, cardiovascular and cerebrovascular disorders, and other conditions [1, 2]. Despite the observed beneficial effects across various diseases, the underlying mechanism remains largely unknown.

Aralia stipulata Franch., also known as *A. taibaiensis* Z.Z. Wang et H.C. Zheng (verified in "The World Flora Online" on July 30, 2023) is a species of *Aralia* widely distributed in the mountainous regions of central and western China, particularly in the Qinba Mountains. In this region, it is commonly referred to as *Flying centipede seven*, classified as one of the *Seven Medicines of Tai Bai*, and documented in the "Taibai Mountain Botanical Records". Traditional medicine has employed this plant in the treatment of diabetes, gastropathy, rheumatism, and cardiovascular diseases [3]. The principal bioactive compounds in *A. taibaiensis* are triterpenoid saponins, which have demonstrated significant antioxidant and antiglycation properties (similar to those found in ginseng, *Eleutherococcus senticosus*, pseudoginseng, and related plants) [4], as well as the ability to improve mitochondrial function [5] and promote angiogenesis [6]. In a previous study, we demonstrated that saponins from *A. taibaiensis* (sAT) offered protection against ischemia/reperfusion (I/R)-induced brain injuries and confirmed that sAT modulated the protein kinase B (Akt)/sirtuin 1 (SIRT1)/forkhead box O3 protein (FOXO3a)/peroxisome proliferator-activated receptor-γ coactivator-1α (PGC-1α) pathway to enhance mitochondrial function [7]. However, the precise mechanisms by which sAT regulates the Akt pathway and the potential protein transduction contributing to these protective effects remain to be elucidated.

Ischaemic stroke (IS) is one of the leading causes of death worldwide. Currently, tissue-type plasminogen activator (tPA) is the only proven effective treatment for IS [8, 9]. However, due to its narrow time window and other side effects, it is necessary to discover new medicines for the treatment of IS [10]. In our research and other studies, oxidative stress and mitochondrial dysfunction

* Corresponding author.
E-mail address: duanjl@nwpu.edu.cn
Δ These authors contributed equally to this work.

https://doi.org/10.1016/S1875-5364(25)60841-7

have been verified to play important roles in the development of IS [7, 11]. Although many agents have shown beneficial effects against IS in animal models, most have proven ineffective in clinical trials. In brain tissue, apelin/apelin receptors (ARs) are widely distributed and play important roles in regulating blood pressure, appetite, angiogenesis, and other functions [12-14]. Our previous research has demonstrated that apelin 13,with greater potency than other apelin isoforms, protects against ischemia-induced brain oxidative stress and mitochondrial dysfunction by regulating the adenosine 5'-monophosphate (AMP)-activated protein kinase (AMPK)-mediated antioxidant pathway [5]. Although its neuroprotective effects have been demonstrated in many animal experiments, the poor stability, difficulty in clinical administration, and high invasiveness of apelin 13 have limited its use to intraventricular injection [6, 15, 16]. To harness the neuroprotective effects of apelin 13, it is necessary to identify chemicals or herbal components that can activate the apelin/AR in the brain.

Given the comparable pharmacodynamic effects of sAT and apelin 13 in ameliorating mitochondrial dysfunction in the brain ischemia/reperfusion (I/R) model, we hypothesized that sAT might influence the expression of apelin 13. Preliminary experiments supported this hypothesis. However, the precise role of apelin 13 in mediating the effects of sAT remains to be elucidated. The mechanism by which sAT regulates apelin 13 in the brain is not yet fully understood. This study aims to address these questions and provide experimental evidence for the potential therapeutic application of sAT and targeted chemical compounds of apelin/AR in ischemic brain injury.

2. Materials and Methods

2.1. Materials

Fetal bovine serum (FBS) was obtained from Zhejiang Sijiqing Biotechnology Co., Ltd. (Hangzhou, China). Penicillin–streptomycin solution and Dulbecco's Modified Eagle's medium (DMEM) were procured from HyClone (Logan, UT, USA). JC-1, TTC, SB203580, anisomycin, and dihydroethidium (DHE) were acquired from Sigma–Aldrich Co. (St. Louis, USA). A fluorescent terminal deoxynucleotidyl transferase-mediated dUTP nick end labeling (TUNEL) staining kit was sourced from Roche (Germany). ATP, 4-Hydroxynonenal (4-HNE), 8-hydroxy-2'-deoxyguanosine (8-OHdG), and nitrotyrosine measurement kits were obtained from Jiancheng Biotechnology (Hangzhou, China). s-100β Elisa kit was purchased from Signalway Antibody (Nanjing, China). anti-P-P38 mitogen-activated protein kinase (P38 MAPK), Anti-UCP2, anti-SOD2, anti-TAFM, anti-P38 MAPK, anti-ATF4, anti-hypoxia-inducible factor-1α (HIF-1α), anti-P-FOXO3a, anti-FOXO3a, anti-P-PGC-1α, anti-P-Akt, anti-PGC-1α, anti-SIRT1, anti-AMPK, anti-Akt, anti-P-AMPK, anti-UCP2, anti-SOD2, anti-NRF1, anti-acetylated lysine, and anti-*β*-actin primary antibodies were acquired from Cell Signaling Technology (Beverly, MA, USA). Apelin and AR primary antibodies were obtained from Abcam (USA). Translocase of outer mitochondrial membrane 20 (TOMM20), cytochrome c oxidase subunit I (COX I), and cytochrome c oxidase subunit IV isoform 1 (COX IV) primary antibodies were sourced from Proteintech (Wuhan, China). Secondary antibodies (Goat anti-rabbit, Goat anti-rat) were procured from Boster Biological Technology (Wuhan, China). Lipofectamine 3000 reagent was obtained from Life Technologies (CA, USA). Sodium dodecyl sulfate-polyacrylamide gel electrophoresis (SDS-PAGE) gel preparation kits and bicinchoninic acid assay (BCA) protein assay kits were acquired from Solarbio (Beijing, China). The quantitative reverse transcription polymerase chain reaction (qRT-PCR) kit was obtained from Takara Bio (Japan). All other chemicals used were of the highest purity grade commercially available.

2.2. Preparation of sAT and high-performance liquid chromatography (HPLC) analysis

The root bark of *A. taibaiensis* was collected from Mountain Taibai, Meixian, Shaanxi Province, China. Initially, dried root bark (100 g) was ground into powder and extracted three times with 10-fold (*V*/*V*) 80% ethanol under reflux for 1 h each time. Subsequently, the ethanol extract was concentrated and suspended in distilled water, followed by three separate fractionations using 3-fold (*V*/*V*) *n*-butanol saturated with water. Finally, the *n*-butanol extracts were combined and evaporated using a rotary evaporator at 60 °C [17]. The yield of sAT was 10.57% (*W*/*W*). Aralosode A, stipuleanoside R2, aralosode C, chikusetsusaponin IVa, pseudoginsenoside RT1, and tarasaponin IV were commercially obtained from Baoji Herbest Bio-Technology Co., Ltd., with a purity exceeding 98%.

To analyze the contents in sAT, a Waters e2695 alliance HPLC separations module equipped with a PFchrom EP C18 chromatographic column (4.6 nm × 250 nm, 5 μm, 120 A) at 30 °C was utilized. The UV absorbance of the samples was measured at 203 nm. The mobile phase composition employed solvent A (acetonitrile) and solvent B (0.1% phosphoric acid aqueous solution). The gradient program was established as follows: 0–10 min: 5%–20% A, 10–25 min: 20%–28% A, 25–35 min: 28%–33% A, 35–45 min: 33%–38% A, 45–55 min: 38%–46% A, 55–60 min: 46%–60% A, 60–70 min: 60%–75% A, 70–80 min: 75%–45% A, 80–90 min: 45%–5% A. A sample volume of 10 μL of the sAT solution was injected into the HPLC system, with the flow rate set at 0.8 mL·min^{-1}.

2.3. Animals cerebral ischemia model and drug administration

Male C57BL/6 mice, aged 5–6 weeks (22–25 g), and male Sprague Dawley rats, aged 3 months (200–230 g), were obtained from the Experimental Animal Center of the Fourth Military Medical University. Animals were provided ad libitum access to water and food and housed in a standardized facility with controlled temperature (22–25 °C), humidity (45%–50%), and a 12-h light/dark cycle. The protocols were approved by the Ethics Committee for Animal Experimentation of the Northwestern Polytechnical University. All animal experiments were conducted in accordance with the Guidelines for Animal Experimentation of the Northwestern Polytechnical University and the Guide for the Care and Use of Laboratory Animals, 8th edition, 2011 (No. 202101118).

Animals were anesthetized with chloral hydrate (400 mg·kg^{-1}, i.p.). Under an *in vivo* microscope, the right common carotid artery (CCA) and external carotid artery (ECA) were exposed. The internal carotid artery (ICA) was incised up to the middle cerebral artery. Subsequently, the ECA end was ligated with a surgical suture, and the CCA was permanently occluded with a microvascular clamp while temporarily occluding the ICA. A small incision was then made on the ECA, and a nylon thread (diameter: 0.36 mm) was inserted. The nylon thread was carefully and slowly advanced through the ICA until slight resistance was felt, indicating that the tip had wedged into the origin of the anterior cerebral artery, resulting in cerebral artery occlusion. After 1.5 h of ischemia induction, the nylon thread was slowly removed [18]. Subsequently, animals were administered three different doses of sAT at low, medium, and high levels, corresponding to 80, 160, and 320 mg·kg^{-1}, respectively. Both the control group and the model group were administered the same volume of saline.

2.4. Behavioral–Rotarod test

Upon setting the rotation speed and connecting the power supply, the wheel initiates automatic rotation. The rotational speed incrementally increases from 2 to 50 r·min^{-1} over a 5-minute duration. The mice undergo initial training to acclimate to

the wheel, followed by three successive 5-minute experiments. A 30-minute rest period is provided between each experiment. The time intervals and rotational speeds at which the mice lose balance and fall from the rotating rod during the final three experiments are documented for subsequent analysis. 2.5 HE, Nissl staining, Immunohistochemistry and Immunofluorescence.

2.5. Haematoxylin and eosin (HE), Nissl staining, Immunohistochemistry and Immunofluorescence

Brain tissues were prepared and fixed in 4% paraformaldehyde for 24 h, followed by embedding in paraffin and sectioning into slices 4 μm slices. The brain sections underwent HE or Nissl staining according to standard protocols and were examined using an optical microscope (Olympus, Japan).

For immunohistochemistry, the tissue sections underwent treatment with xylene, varying concentrations of alcohol, and 1% H_2O_2. Antigen retrieval was conducted by heating at 95 °C for 10 min. Subsequently, the sections were incubated with primary antibodies against TOMM20 (1∶200), COX I (1∶200), COX IV (1∶200), SOD2 (1∶200), and mitochondrial transcription factor A (TFAM) (1∶200) at 4 °C for 12 h. This was followed by incubation with secondary antibodies for 30 min and streptavidin-peroxidase for an additional 40 min. The stained sections were then examined using an optical microscope (Olympus, Japan).

For immunofluorescence, the sections were incubated with anti-apelin13 (1∶200), AR (1∶200), and ZO-1 (1∶200) antibodies at 4 °C for 12 h. Subsequently, the sections were incubated with fluorescent secondary antibodies for 30 min. The stained sections were then observed using a laser scanning confocal microscope (Nikon, Japan).

2.6. TUNEL staining

TUNEL staining was employed to identify apoptotic cells in the ischaemic penumbra. A fluorescent TUNEL staining kit (Roche, Germany) was utilized following the manufacturer's protocol. The sections were incubated with a TUNEL reagent mixture and 4',6-diamidino-2-phenylindole (DAPI) at 37 °C for 30 min, then examined using a laser scanning confocal microscope (Nikon, Japan).

2.7. Quantification of s-100β in serum

The serum s-100β levels were quantified using a Mouse Protein S100-β ELISA Kit (Signalway Antibody). Serum samples were collected using serum separation tubes (SST), allowing the blood to clot for 30 min before centrifugation at approximately 1000 × *g* for 15 min. A 100 μL aliquot of serum was used for analysis. The optical density of each well was immediately measured using a microplate reader set to 450 nm wavelength.

2.8. Quantification of ATP in brain tissues

The ATP levels in the ischaemic penumbra were quantified using an ATP measurement kit (Beyotime Biotechnology). Ischaemic penumbra tissues (20 mg) were harvested, lysed, and subsequently centrifuged at 4 °C and 12 000 × *g* for 5 min. The resulting supernatant was collected for further analysis. An ATP standard curve was generated, and the ATP content in the sample was determined based on this standard curve.

2.9. Quantification of ROS in brain tissues

I/R stimulates the generation of reactive oxygen species (ROS) and leads to the peroxidation of lipids, DNA, and proteins. DHE is a reagent employed to detect the presence of ROS. 4-HNE is a product of lipid peroxidation, 8-OHdG is a DNA oxidation product, and nitrotyrosine is a protein oxidation product. These markers are quantified in the ischemic penumbra region following the manufacturer's protocol.

2.10. Cell culture and treatments

In vitro experiments were conducted using the mouse hippocampal neuronal cell line, HT22 cells. The cells were cultured in DMEM containing 10% fetal bovine serum and antibiotics (penicillin, 100 IU·mL^{-1}; streptomycin, 100 μg·mL^{-1}) at 37 °C in a humidified incubator with 5% CO_2 [7]. SB203580 (1 μmol·L^{-1}) and anisomycin (1 μmol·L^{-1}) were applied in conjunction with sAT to HT22 cells for 24 h, followed by incubation with Earle's balanced salt solution (116 mmol·L^{-1} NaCl, 5.4 mmol·L^{-1} KCl, 0.8 mmol·L^{-1} $MgSO_4$, 1 mmol·L^{-1} NaH_2PO_4, 0.9 mmol·L^{-1} $CaCl_2$, and 10 mg·L^{-1} phenol red) in a hypoxia chamber (Thermo Scientific, USA) containing a gas mixture of 95% N2 and 5% CO_2 for 3 h. Then, the cells were treated with the normal culture medium with or without sAT at doses of 15, 30, and 60 μg·mL^{-1}, and SB203580 (1 μmol·L^{-1}) or anisomycin (1 μmol·L^{-1}) for 6 h to imitate the reperfusion process. The cells treated under normal conditions serve as the control group.

2.11. siRNA transfection

The overexpression lentiviruses for activating transcription factor 4 (ATF4) and the small interfering RNA (siRNA) plasmids for AR, ATF4, and HIF-1α were acquired from Santa Cruz Biotechnology. Transfection was conducted using Lipofectamine 3000 reagent for 48 h, and the transfection efficiency was verified by Western blotting. Subsequently, the transfected cells were utilized in relevant experiments.

2.12. DHE staining and JC-1 staining

Following various treatments, the cells underwent staining with dihydroethidium (DHE, 1 μmol·L^{-1}) and JC-1 (2 μmol·L^{-1}) for 20 min. The stained cells were then observed using a laser scanning confocal microscope (Nikon, Japan).

2.13. Western blotting

Proteins from brain tissues and HT22 cells (30 μg) were separated using SDS-PAGE and transferred onto polyvinylidene fluoride (PVDF) membranes, followed by blocking for 1 h. The membranes were incubated with primary antibodies at 4 °C overnight and with secondary antibodies (1∶5000) for an additional 30 min. Subsequently, the membranes were visualized using an enhanced chemiluminescence (ECL) kit and scanned by image-analysis systems (Bio-Rad, USA).

2.14. Statistical analysis

Data are presented as the mean ± standard deviation. Statistical analysis was conducted using GraphPad Software (GraphPad Prism 5.0 Inc., La Jolla, CA), employing one-way ANOVA followed by Tukey's test. A P value < 0.05 was considered statistically significant.

3. Results

3.1. Analysis of the main saponins in sAT

The chromatogram of the primary components of the mixed reference standard and saponins of sAT was obtained through HPLC following the methodology described in the Methods section (Figs. 1A and 1B). The saponin composition in sAT was identified using Chikusetsu saponin IVa, stipuleanoside R2, pseudo-

ginsenoside RT1, araloside A, tarasaponin IV, and araloside C standard substances to determine the chromatographic peak and retention time (Supplemental result. Fig. S1). The retention time of tarasaponin IV was 42.618 min, with a content in sAT of 109.8 mg·g^{-1}. Araloside C had a retention time of 43.117 min and a content in sAT of 338.9 mg·g^{-1}. Stipuleanoside R2 exhibited a retention time of 44.064 min, with its content in sAT being 197.5 mg·g^{-1}. Pseudoginsenoside RT1 showed a retention time of 46.475 min, with a content in sAT of 19.6 mg·g^{-1}. Araloside A had a retention time of 47.409 min and a content in sAT of 92.9 mg·g^{-1}. Lastly, chikusetsu saponin IVa demonstrated a retention time of 49.52 min, with a content in sAT of 1.39 mg·g^{-1}.

3.2. sAT mitigated the brain injuries induced by middle cerebral artery occlusion/reperfusion (MCAO/R)

Our previous study indicated the protective effects of sAT through decreased infarct size and improved neural deficit scores. To further validate these neuroprotective effects, we conducted behavioral experiments, quantified serum s-100β levels, and performed HE and Nissl staining. The elevated s-100β levels in the serum of the MCAO/R group indicated severe nerve damage. However, sAT treatment significantly mitigated MCAO/R-induced nerve injury (Fig. 2A). In behavioral experiments, mice in the MCAO/R group exhibited shorter latency to fall and slower speed at fall. Conversely, mice in the sAT treatment group demonstrated significantly longer latency to fall and higher speed at fall compared to the MCAO/R group (Figs. 2B and 2C). HE staining revealed inflammatory infiltration in brain tissue in the MCAO/R group, with immune cell infiltration and/or microglial activation observed in the ischaemic penumbra (Fig. 2D). In the sAT treatment groups, particularly the high-dose group, neuronal morphology improved, and inflammatory infiltrations de-

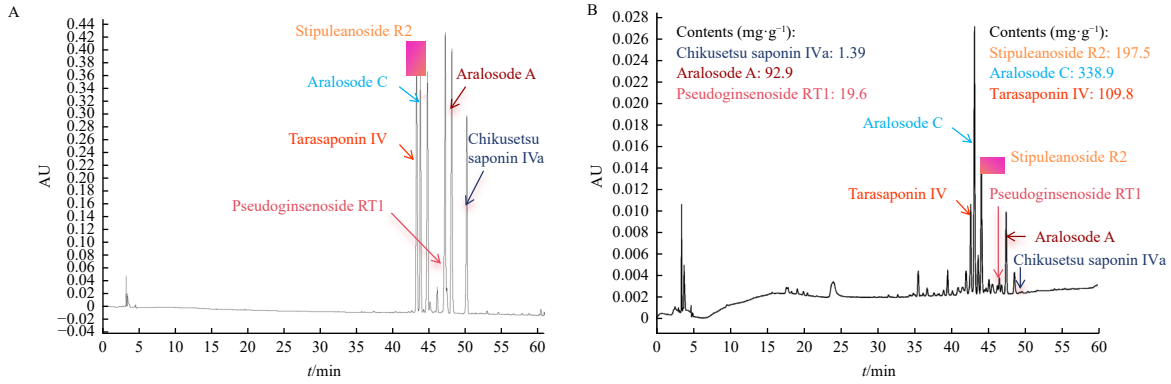

Fig. 1 The primary saponins of sAT. A. HPLC profiles of standard substances. B. HPLC profiles of sAT.

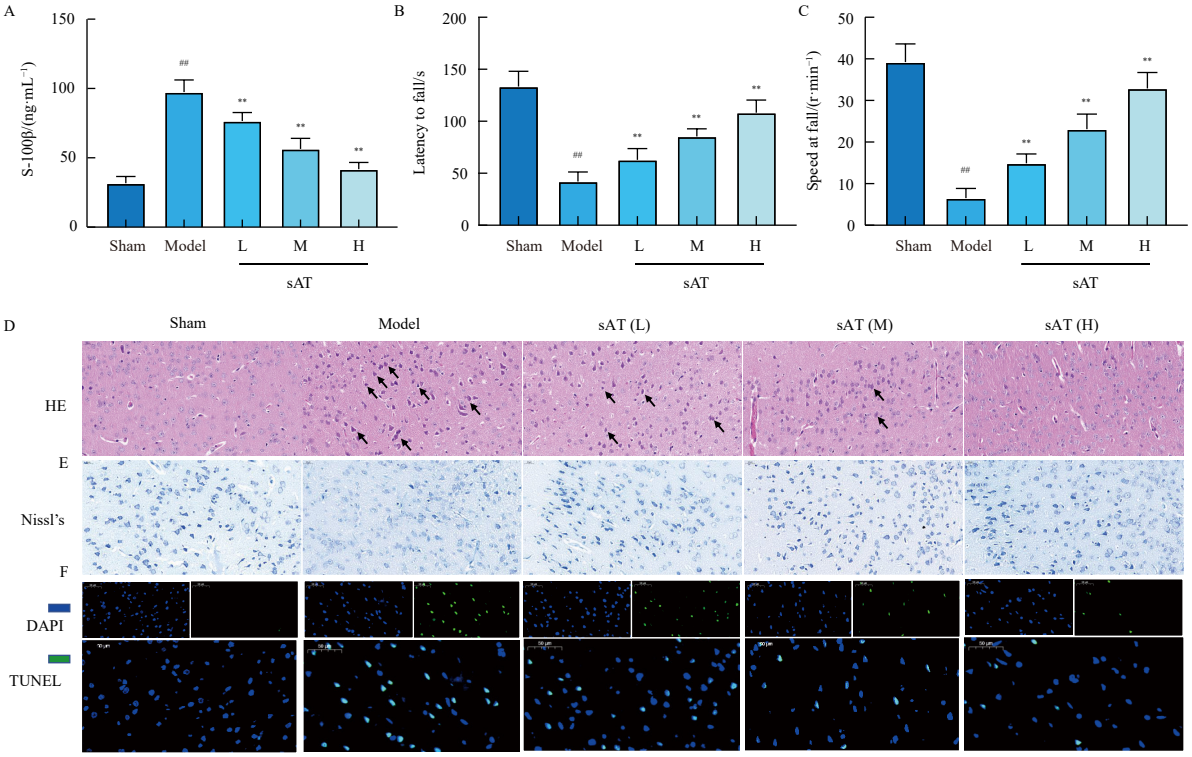

Fig. 2 sAT protected the brain from I/R-induced injuries. A. The content of s-100β was measured using an ELISA assay kit. B. The results of the rota-rod test (the latency to fall). C. The results of the rota-rod test (the speed at fall). D. The HE staining treated with different doses of SAT (× 400 magnification). Black arrows indicate ambiguous structures and nuclear shrinkage. E. Nissl staining treated with different doses of SAT (× 400 magnification). F. TUNEL and DAPI double staining to detect sAT treatment inhibited the MCAO/R induced brain injuries (× 400 magnification). The columns and error bars represent the means ± SDs (n = 5). $^{\#\#}P < 0\ 01$ *vs* the sham group; $^{**}P < 0.01$ *vs* the model group.

creased significantly. Nissl staining results also showed that MCAO/R induced neuronal injury characterized by shrunken cell bodies and pyknotic nuclei (Fig. 2E). sAT treatment significantly improved neuron cell morphology and decreased the number of injured neurons. TUNEL staining, which indicates cell apoptosis rate in the ischaemic penumbra induced by MCAO/R, showed approximately 60% of cells stained with TUNEL and DAPI in Fig. 2F, there were about 60% cells stained with TUNEL and DAPI, indicating massive apoptosis in these sections. In the sAT treatment group, TUNEL-positive staining cell numbers were significantly reduced. These results demonstrate that sAT treatment inhibited MCAO/R-induced brain injuries.

3.3. sAT improved mitochondrial functions

Oxidative phosphorylation is the primary function of mitochondria; thus, related indicators were measured to assess mitochondrial function. TOMM20, COX I, COX IV, SOD2, and TFAM play crucial roles in ATP production and membrane potential maintenance, serving as markers of mitochondrial function [19]. In the ischaemic penumbra of the MCAO/R group, TOMM20 expression levels were decreased, and sAT treatment significantly elevated the expression levels of TOMM20 (Fig. 3A). The immunohistochemical results for COX I, COX IV, SOD2, and TFAM demonstrated that sAT increased their expressions, which were diminished by MCAO/R operation (Figs. 3B–3E). MCAO/R treatment significantly reduced ATP levels, while sAT increased ATP levels in a dose-dependent manner (Fig. 3G). These findings indicate that sAT ameliorated the mitochondrial dysfunction induced by MCAO/R.

DHE staining results demonstrated the inhibitory effect of sAT on ROS production (Fig. 3F). The extent of oxidative stress was assessed by measuring the levels of 4-HNE, 8-OHdG, and nitrotyrosine. The results indicated that MCAO/R operation increased the production of 4-HNE (Fig. 3H), 8-OHdG, and nitrotyrosine (Fig. 3I), suggesting that MCAO/R induced lipid, DNA, and protein oxidation in brain tissues. Following sAT treatment, the levels of ROS, 4-HNE, 8-OHdG, and nitrotyrosine were all reduced, indicating that sAT exhibited anti-oxidative properties.

3.4. sAT protected MCAO/R-induced brain injury through apelin/AR

To investigate the effects of sAT on the apelin system and its potential role in sAT's neuroprotective effects, mRNA and protein expression levels of apelin and its ARs were measured in HT22 cells and brain tissue. The mRNA levels of apelin and AR were both significantly reduced in the oxygen-glucose deprivation/reperfusion (OGD/R) treatment group, while apelin protein levels were significantly decreased. Following sAT treatment, apelin 13 and AR mRNA levels increased significantly, and the protein levels of apelin increased in a dose-dependent manner (Figs. 4A–4D). Similar results were observed in the MACO/R-induced brain injury model (Figs. 4E–4H). These findings suggest that sAT can induce the expression of apelin 13 and the AR brain cells.

To confirm whether apelin 13 mediates the protective effects of sAT during MCAO/R, (Ala13)-Apelin-13 (F13A) was employed. As illustrated in Fig. 4I, F13A treatment significantly negated the inhibitory effect of sAT on cerebral infarction. F13A administration also counteracted the effects of sAT on neurological deficit scores (Fig. 4J) and NSE levels (Fig. 4K). In Fig. 4L, the ZO-1 immunofluorescence in the sAT group appeared bright and uniformly distributed. However, in the F13A + sAT treatment group, the level of ZO-1 was reduced, and its integrity was compromised. Tuj1, a biomarker of neurons, showed lower expression levels in the F13A group compared to the sAT treatment group. The TUNEL staining results (Fig. 4M) also revealed a higher number of apoptotic cells in the ischemic penumbra of the F13A + sAT treatment group compared to the sAT group ($P < 0.01$). In Fig. 4N, compared with the sAT group, TOM20, SOD2, and TFAM immunohistochemical results demonstrated lower levels in the F13A + sAT treatment group. These findings indicate that apelin 13 plays a crucial role in mediating the neuroprotective effects of sAT.

3.5. Regulatory effects of sAT on AMPK/Akt occurred through apelin/AR

In previous studies, we demonstrated that sAT induced AMPK and Akt phosphorylation in the myocardium; however, the mechanism by which sAT activates these pathways remained unclear. To elucidate whether sAT regulated Akt through AMPK, Compound C (a selective AMPK inhibitor, 10 μmol·L^{-1}) was used in combination with sAT. Compared to the sAT treatment group, the phosphorylation level of Akt was significantly reduced by Compound C (Fig. 5A). To determine whether sAT regulated AMPK through Akt, LY294002 (a selective Akt inhibitor, 20 μmol·L^{-1}) was used in combination with sAT. Compared to the sAT treatment group, the phosphorylation level of AMPK was significantly reduced by LY294002 (Fig. 5B). These results indicated a crosstalk relationship between AMPK and Akt during sAT treatment. To verify whether sAT induced the activation of AMPK/Akt through apelin/AR, siRNA targeting AR was used to knock down AR expression (Fig. 5C). Compared to the scrb + sAT group, siAR abolished the AMPK and Akt phosphorylation induced by sAT in brain cells subjected to OGD/R (Fig. 5D). These findings suggest that sAT activates AMPK/Akt through apelin/AR.

3.6. siAR transfection inhibited the protective effect of sAT

To further elucidate the regulatory effects of sAT on AMPK/Akt, potentially mediated through apelin/AR, the downstream effectors of AMPK/Akt were examined. Compared to the scrb + sAT group, PGC-1α and FOXO3a phosphorylation levels, which were elevated by sAT treatments, were diminished by siAR treatment. SIRT1, another downstream target of Akt with deacetylation capabilities, was also reduced by siAR transfection (Fig. 6A). In comparison to the OGD/R + sAT group, CAT, SOD2, NRF1, and UCP2, which are downstream of PGC-1α and FOXO3a, were decreased in the sAT + siAR group (Fig. 6B). The acetylation levels of PGC-1α and FOXO3a, regulated by SIRT1, were significantly increased by siAR treatment (Fig. 6C). Moreover, siAR transfection significantly negated the protective effect of sAT on cell viability (Fig. 6D) and ATP production (Fig. 6E). siAR also promoted ROS production (Fig. 6F) and increased the mitochondrial membrane potential (Fig. 6G), indicating that the protective effects of sAT against oxidative stress and mitochondrial dysfunction were mediated by apelin/AR. These findings suggest that sAT induced AMPK/Akt activation to counter oxidative stress and mitochondrial dysfunction *via* the apelin/AR pathway.

3.7. sAT regulated apelin expression partly by inhibiting P38 MAPK/ATF

P38 MAPK/ATF4 exhibits an opposing regulatory effect on apelin expression. To investigate whether sAT induced apelin expression by inhibiting p38 MAPK/ATF4, the phosphorylation level of p38 MAPK and ATF4 protein expression were assessed. As illustrated in Figs. 7A and 7B, p-p38 MAPK and ATF4 levels were elevated by MCAO/R treatment in animals or OGD/R treatment in HT22 cells. These alterations were mitigated by sAT, demonstrating its inhibitory effects on p38 MAPK/ATF4. To con-

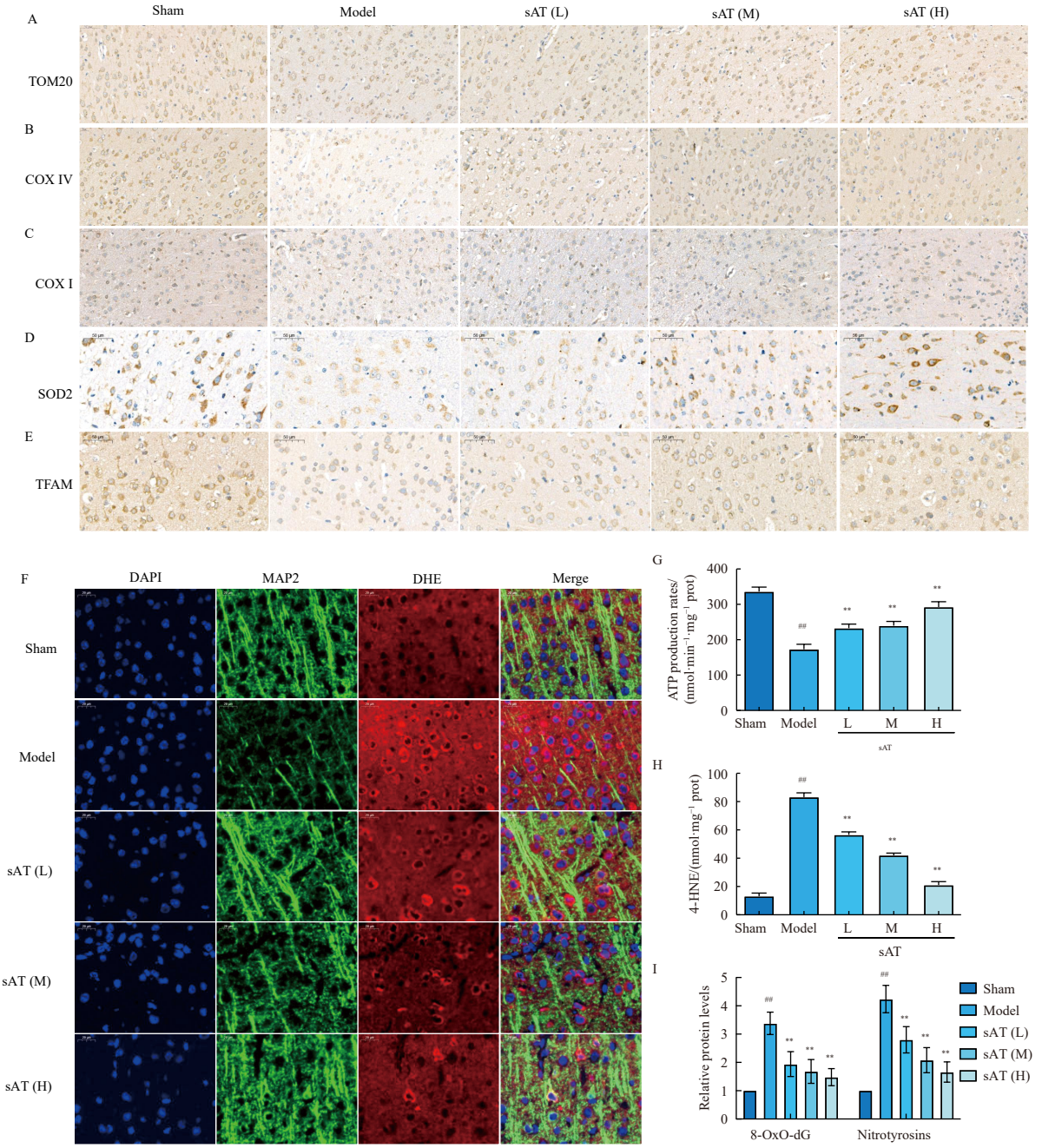

Fig. 3 sAT ameliorated mitochondrial dysfunction and oxidative stress in the brain. The effects of SAT on the expressions of TOMM20 (A), COX IV (B), COX I (C) SOD2 (D) and TFAM (E) in mice brain tissues. F. DHE, MAP2, and DAPI co-staining to visualize the inhibitory effect of sAT treatment on ROS levels induced by MCAO/R. (× 400 magnification). G. ATP levels were quantified using commercial kits. H. 4-HNE levels. I. 8-OHdG levels and Nitrotyrosine levels. The columns and error bars represent the means ± SDs (n = 5). $^{\#\#}P < 0.01$ *vs* the sham group; $^{**}P < 0.01$ *vs* model.

firm the regulatory effect of p38 MAPK on apelin expression, an inhibitor of p38 MAPK, SB203580, and an activator of p38 MAPK, anisomycin, were employed. Fig. 7C shows that SB203580 treatment decreased p-p38 MAPK and ATF4 expression levels while increasing apelin 13 expression; conversely, anisomycin increased p-p38 MAPK and ATF4 expression levels while reducing apelin 13 expression. SB203580 (an inhibitor of p38 MAPK, 1 μmol·L^{-1}) and anisomycin (an activator of p38 MAPK, 1 μmol·L^{-1}) were co-cultured with sAT to verify the role of p38 MAPK in sAT-mediated regulation of apelin 13. As shown in Fig. 7D, compared to the sAT treatment group, the anisomycin + sAT group exhibited lower levels of apelin 13 expression and higher levels of ATF4 expression, while the SB203580 + sAT treatment increased apelin 13 and decreased ATF4 expression levels.

Subsequently, the regulatory effects of ATF4 on apelin expression were confirmed through siRNA knockdown (Fig. 7E) and ATF4 overexpression experiments. As illustrated in Fig. 7F, siATF4 enhanced the expression of apelin 13, while ATF4 overexpression reduced it, demonstrating that ATF4 suppressed apelin 13 expression in neurons. siATF4 amplified apelin 13 expression in conjunction with sAT effects, whereas ATF4 overexpression significantly diminished sAT-induced apelin 13 expression (Fig. 7G). The cell viability (Fig. 7H) and ATP measurement (Fig. 7I) results further corroborated that siATF4 augmented the protective effects of sAT, while ATF4 overexpression attenuated them. These findings confirmed that sAT increased apelin 13 expression by inhibiting the p38 MAPK/ATF4 pathway (Fig 7J).

3.8. sAT regulated apelin expression partly by activating HIF-1α

HIF-1α is another upstream target of apelin. To investigate whether sAT induced the expression of apelin through HIF-1α,

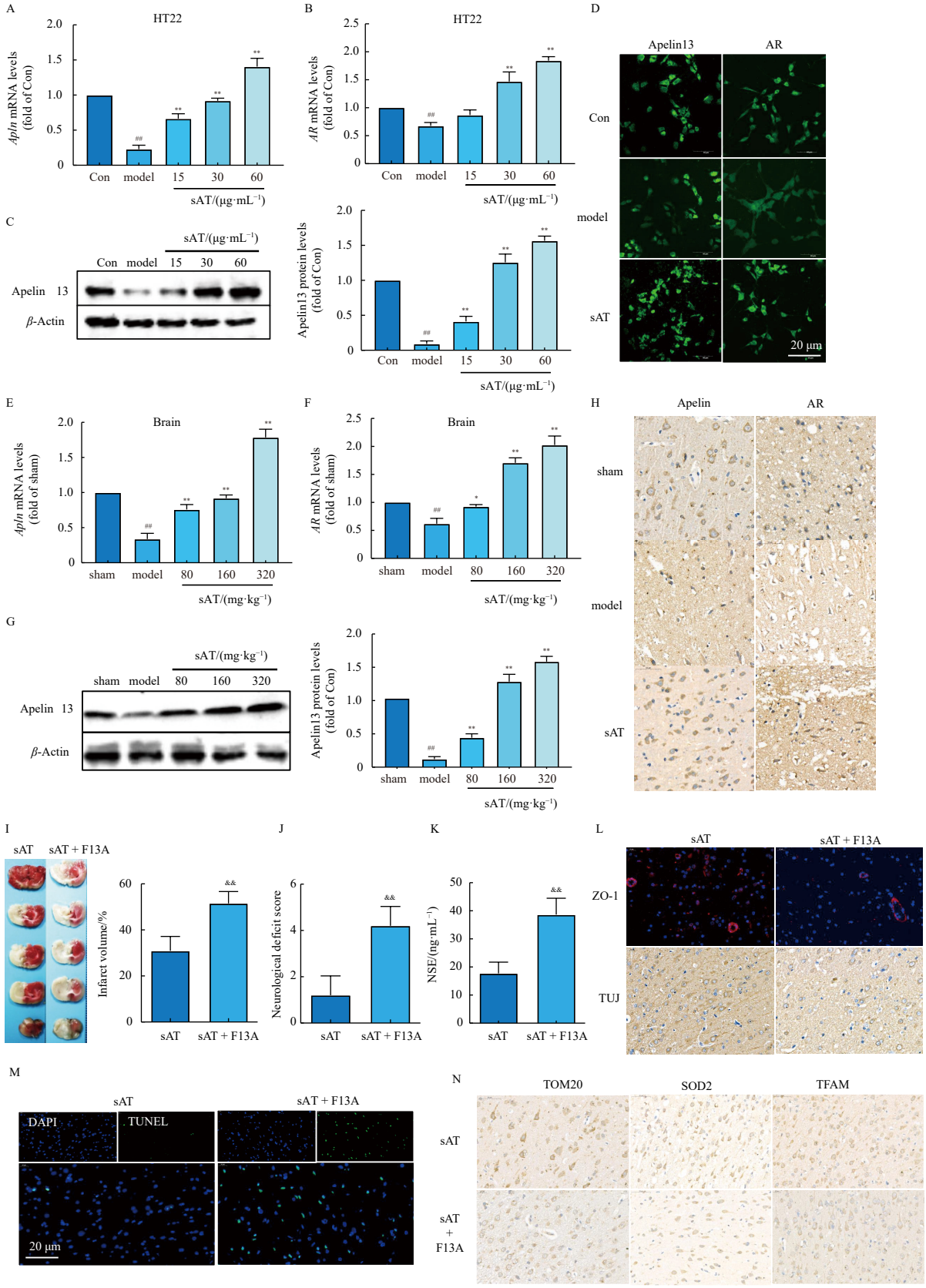

Fig. 4 sAT regulated apelin and AR expressions in HT22 cells and brain tissues. A. QRT-PCR results of the *Apln* gene in HT22 cells; B. QRT-PCR results of the *AR* gene in HT22 cells; C. Protein levels of apelin 13 in HT22 cells. D. Immunofluorescence results of apelin 13 in HT22 cells; E. QRT-PCR results of the *Apln* gene in the brain; F. QRT-PCR results of the *AR* gene in the brain; G. Protein levels of apelin 13 in brain. H. The effects of SAT on the expressions of apelin and ARs. Animals were pretreated with or without F13A (300 μg·kg^{-1}, i.p.) and subjected to MCAO/R. I. TTC staining. J. Neurological scores in rats. K. NSE levels in each group were measured using an NSE measurement kit. L. Protein levels of ZO-1 and TUJ in brain. M. TUNEL staining in the ischaemic penumbra. × 200. N. Protein levels of TOM20, SOD2, and TFAM in the brain. The columns and error bars represent the means ± SDs (n = 3). $^{\#\#}P < 0.01$ *vs* the sham group or Con; $^{*}P < 0.05$, $^{**}P < 0.01$ *vs* model; $^{\&\&}P < 0.01$ *vs* sAT treatment group.

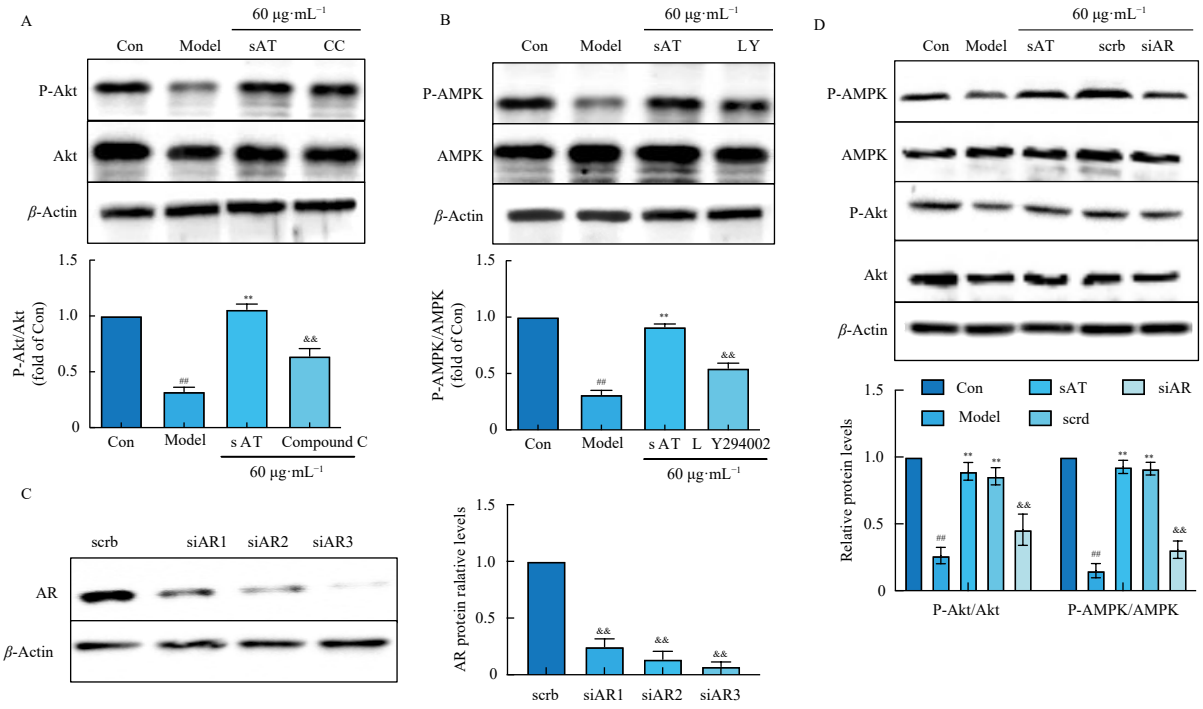

Fig. 5 sAT regulated AMPK/Akt through apelin/AR. A. AMPK inhibitor, Compound C, at a final concentration of 10 μmol·L^{-1} in conjunction with sAT, followed by measurement of the Akt phosphorylation level. B. A selective AMPK inhibitor, LY294002, at a final concentration of 20 μmol·L^{-1} was utilized alongside sAT, after which the AMPK phosphorylation level was assessed. The siRNA plasmid for AR was transfected using Lipofectamine 3000 reagent for 48 h, followed by various treatments. AMPK and Akt expression levels were subsequently measured. C. SiAR diminished AR expression. D. SiAR nullified the effects of sAT on AMPK and AKT phosphorylation levels. The columns and error bars represent the means ± SDs (n = 3). $^{\#\#}P < 0.01$ *vs* Con; $^{**}P < 0.01$ *vs* model; $^{\&\&}P < 0.01$ *vs* sAT treatment group.

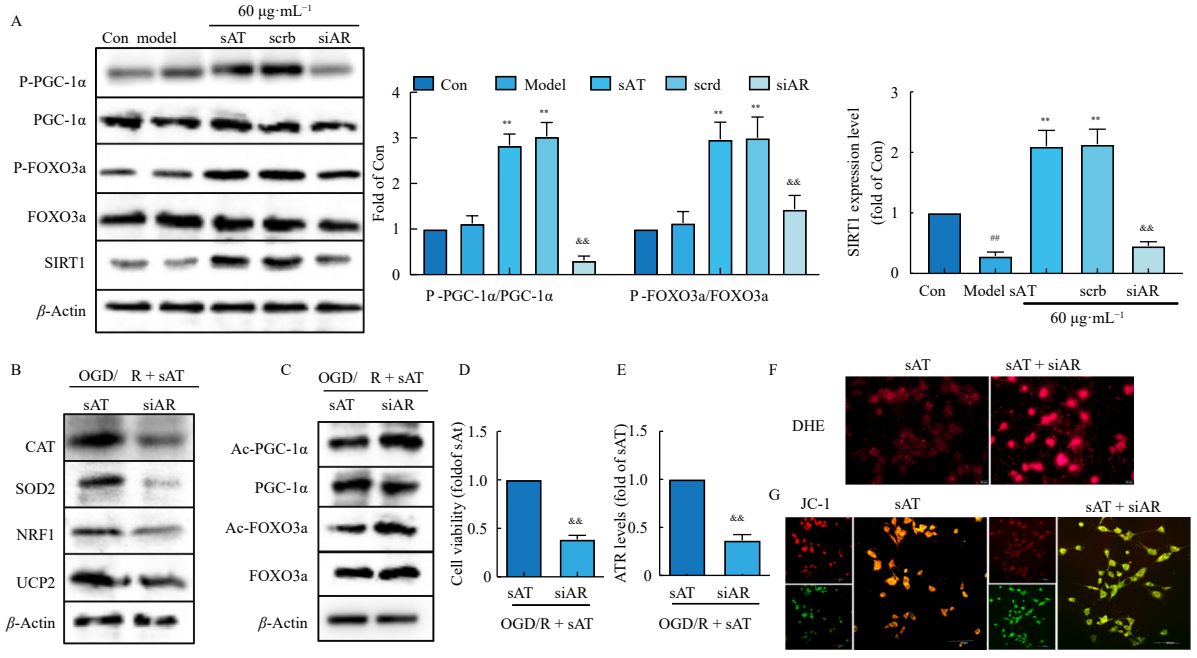

Fig. 6 siAR transfection inhibited the protective effect of sAT. The siRNA plasmid for AR was transfected using Lipofectamine 3000 reagent for 48 h, after which protein expression levels and other indicators were measured following various treatments. A. SiAR negated the effects of sAT on the phosphorylation level of PGC-1α and FOXO3a, as well as SIRT1. B. SiAR counteracted the effects of sAT on the expression of CAT, SOD2, NRF1, and UCP2 downstream of PGC-1α and FOXO3a. C. SiAR neutralized the effects of sAT on the FOXO3a and PGC-1α acetylation levels. D. Cell viability was assessed after different treatments. E. ATP levels. F. DHE staining. × 200. G. JC-1 staining. × 200. The columns and error bars represent the means ± SDs (n= 3). $^{\#\#}P < 0.01$ *vs* Con; $^{**}P < 0.01$ *vs* model; $^{\&\&}P < 0.01$ *vs* sAT treatment group.

HIF-1α protein expression levels were initially assessed. As illustrated in Fig. 8A and B, sAT increased HIF-1α expression levels in the MCAO/R animal model and HT22 cell OGD/R model in a dose-dependent manner. Subsequently, HIF-1α was knocked down using siRNA transfection (Fig. 8C). Compared to the sAT treatment group, siHIF-1α significantly reduced the protein expression levels of apelin 13 (Fig. 8D). Additionally, siHIF-1α significantly diminished the protective effects of sAT on HT22 cells, as evidenced by decreased ATP levels (Fig. 8E), reduced cell viability (Fig. 8F), and increased apoptosis rates (Fig. 8G). An elevated mitochondrial membrane potential, indicated by increased green fluorescence and decreased red fluorescence, was observed in the sAT + siHIF-1α group (Fig. 8H). DHE staining results demonstrated that siHIF-1α negated the inhibitory effect of sAT on ROS

production (Fig. 8I). These findings suggest that sAT regulates apelin 13 expression partly through the upregulation of HIF-1α (Fig. 8J).

4. Discussion

Saponins demonstrate beneficial effects across various tissues by inhibiting inflammation, apoptosis, oxidative stress, and mitochondrial dysfunction [20]. Saponins exert beneficial effects in inhibiting inflammation, apoptosis, oxidative stress, and mitochondrial dysfunction in many tissues [21]. These compounds have shown promise in treating brain-related disorders, including Huntington's disease, stroke, Alzheimer's disease, and Parkinson's disease [22]. Steroidal saponins extracted from Anemarrhena asphodeloides Bunge (sAT) are derived from an edible medicinal plant and exhibit therapeutic potential in metabolic, cardiovascular, and renal diseases [17, 23, 24]. Our previous research revealed that sAT inhibits oxidative stress and mitochondrial dysfunction induced by brain I/R through the Akt/SIRT1 pathway [7]. The present study demonstrates that ARs are involved in sAT-mediated regulation of the AMPK/Akt pathway. Furthermore, P38 MAPK/ATF4 and HIF-1α play crucial roles in this process.

Apelin/AR has demonstrated protective effects against ischemia-induced neural injuries in previous studies, including our own. Our research revealed that apelin 13 inhibits oxidative stress and inflammation in a brain I/R model. Wu *et al.* found that apelin 13 alleviated endoplasmic reticulum (ER) stress in early brain injury following subarachnoid hemorrhage by regulating the AMPK/TXNIP/NLRP3 pathway [25]. Moreover, in a cerebral I/R model, apelin 13 treatment inhibited neuronal apoptosis and autophagy by modulating the Akt pathway [26]. These findings suggest that chemical compounds or drugs regulating apelin/AR may be beneficial for treating neuronal injuries. Based on RNA-Seq results from brain tissue treated with sAT, we hypothesized that

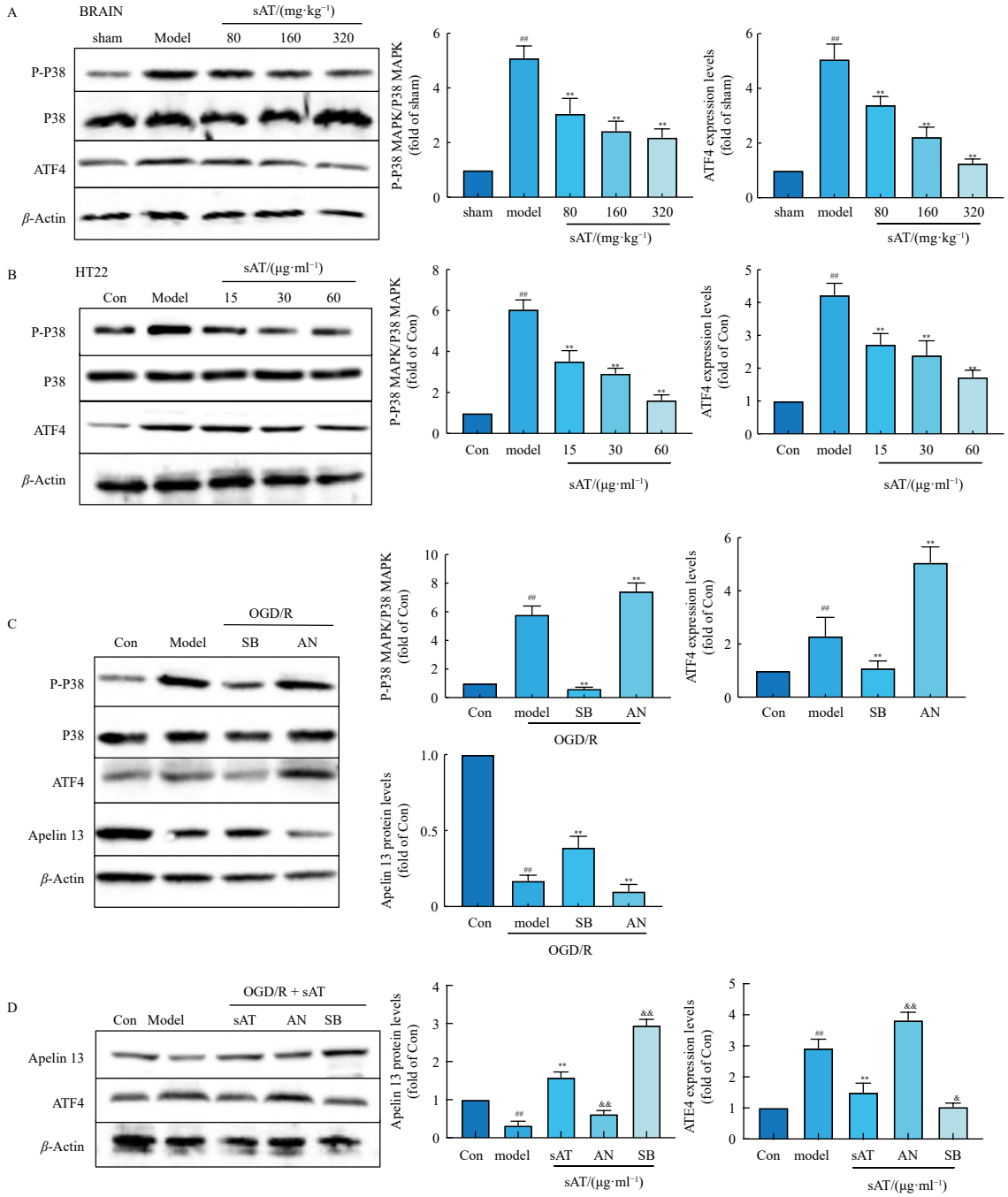

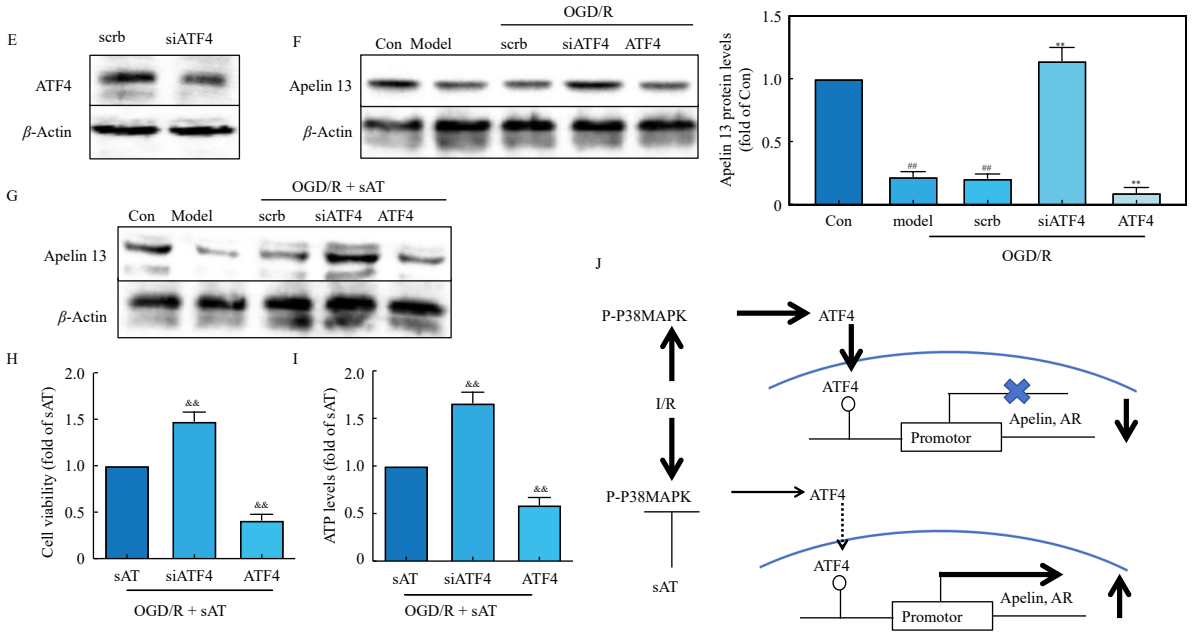

Fig. 7 The effects of sAT on apelin expression were partially mediated by inhibiting P38 MAPK/ATF4. Various doses of sAT inhibited P38 MAPK phosphorylation and ATF4 expression levels in brain tissues (A) and HT22 cells (B). C. In the OGD/R model, HT22 cells were treated with SB203580 (SB, 1 μmol·L^{-1}) and anisomycin (AN, 1 μmol·L^{-1}), and P38 MAPK phosphorylation, apelin, and ATF4 expression levels were assessed. D. HT22 cells were treated with sAT in combination with SB203580 (SB, 1 μmol·L^{-1}) or anisomycin (AN, 1 μmol·L^{-1}), and subsequently, apelin and ATF4 protein expression levels were quantified. E. SiATF4 significantly suppressed the protein expression level of ATF4. F. Knockdown and overexpression of ATF4 significantly modulated Apelin expression in the OGD/R model. G. In the OGD/R model, Apelin expression was measured following simultaneous ATF4 knockdown or overexpression and sAT administration. H. Cell viability was evaluated using CCK8. I. ATP levels were determined using a kit. J. sAT enhanced the expression of apelin 13 by inhibiting p38 MAPK/ATF4. The columns and error bars represent the means ± SDs (n = 3). $^{\#\#}P < 0.01$ *vs* Con; $^{**}P < 0.01$ *vs* model; $^{\&\&}P < 0.01$ *vs* sAT treatment group.

apelin 13 partially contributes to the protective effects of sAT in the brain I/R model. To test this hypothesis, we measured apelin 13 and AR expression levels in animal brain tissues and HT22 cells. As anticipated, sAT promoted the expression of apelin 13 and AR at both protein and mRNA levels in brain tissues and HT22 cells. F13A, an antagonist of AR, negated the neuroprotective effects of sAT. These results indicate that the regulatory effects of sAT on mitochondrial function and oxidative stress might partially occur through the upregulation of Apelin/AR.

Both sAT and apelin/AR demonstrate promotional effects on AMPK and Akt phosphorylation in the cerebral I/R model. To confirm whether sAT regulates AMPK and Akt phosphorylation through the apelin/AR pathway, siAR transfection was performed. The results indicate that siAR abolished the phosphorylation of AMPK and Akt induced by sAT, suggesting that sAT regulates AMPK/Akt potentially through apelin/AR. The SIRT1-mediated anti-oxidative pathway was identified as the downstream of AMPK/Akt [27, 28]. To further confirm the regulatory role of sAT on apelin/AMPK/Akt, the levels of SIRT1 and its downstream targets were measured. SIRT1 is a nicotinamide adenine dinucleotide (NAD)-dependent deacetylase that directly regulates peroxisome proliferator-activated receptors γ coactivator 1a (PGC-1a), an important factor in mitochondrial energy metabolism [29]. When PGC-1α content and activity are inhibited by I/R, it leads to a disorder of mitochondrial energy metabolism in neurons and glia, thus inducing brain injuries [30]. Additionally, SIRT1 also regulates FOXO activity through its deacetylase activity. Previous studies have shown that FOXO3a plays important roles in regulating oxidative stress and mitochondrial energy metabolism by promoting antioxidant protein expression [29]. To confirm whether the protective effects of sAT occur through regulating SIRT1 *via* apelin/AR, their expression and phosphorylation levels were measured. The results showed that sAT upregulated the expression of SIRT1 and the phosphorylation of PGC-1α and FOXO3a. However, siAR abolished the regulatory effects of sAT on SIRT1 expression and PGC-1α and FOXO3a phosphorylation. Additionally, siAR also reversed the protective effects of sAT against oxidative stress and mitochondrial dysfunction. These results suggest that sAT regulates AMPK/Akt/SIRT1 by mediating Apelin/AR.

Subsequently, we sought to elucidate the specific protein or pathway involved in the regulatory effects of sAT on apelin/AR. Previous research has shown that apelin/AR is transiently regulated by I/R [31]. Ischemia and glucose deprivation have been found to induce the expression of Apelin and AR in the early stages by increasing HIF-1α [32]. The promoter regions of the Apelin and AR genes are situated within regulation regions of hypoxia response elements (HREs). When HIF-1α is activated and binds to HREs, it triggers the transcriptional expression of apelin and AR [33]. In the later stages of ischemia, secondary injury factors (such as oxidative stress and inflammation) have been observed to reduce apelin and AR expression [31]. Given these findings, we investigated the regulatory effect of sAT on HIF-1α. Our results demonstrated that sAT increased HIF-1α protein expression levels in both brain tissues and HT22 cells. Notably, knockdown of HIF-1α by siRNA significantly attenuated the expression of apelin 13, which had been upregulated by sAT. Moreover, the protective effects of sAT on mitochondrial dysfunction and oxidative stress were also inhibited by siHIF-1α. These findings suggest that sAT upregulates apelin expression, at least in part, through the induction of HIF-1α.

Following ischemia, reperfusion induces a reduction in Apelin/AR. During reperfusion, the secondary inflammatory response inhibits apelin and AR expression by directly targeting the apelin gene promoter and downregulating its expression [34]. ER stress is a major factor in I/R injury and is activated only during the brain reperfusion stage [35]. ATF4, regulated by p38 MAPK, plays a crucial role as a transcription factor in regulating apelin expression within the ER [36]. Within the apelin promoter, the CCAAT/enhancer-binding protein-b (C/EBP-b) sites are bound by ATF4, resulting in reduced expression of apelin [37]. As the main saponin component in sAT demonstrated inhibitory effects on the P38 MAPK pathway in LPS-stimulated THP-1 cells [38], we hypothesized that sAT induces apelin expression by inhibiting P38

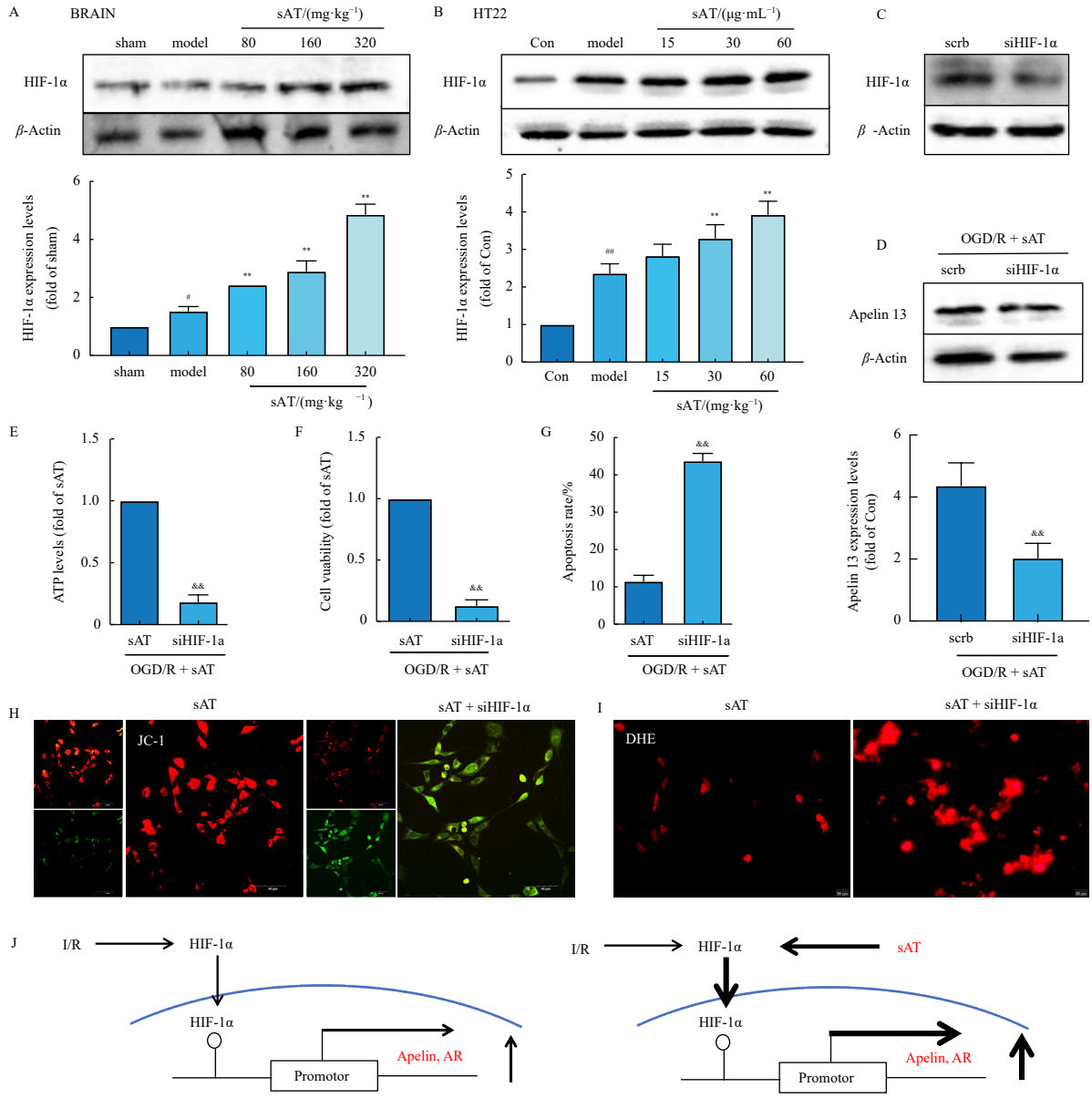

Fig. 8 The effects of sAT on apelin expression were partially mediated through HIF-1α induction. Varying concentrations of sAT increased HIF-1α expression levels in brain tissues (A) and HT22 cells (B). C. SiHIF-1α significantly reduced the protein expression level of HIF-1α. D. HT22 cells were transfected with siHIF-1α and subsequently treated with sAT and OGD/R. Apelin 13 protein levels were measured after different treatments. E. ATP levels were assessed in the sAT and sAT + siHIF-1α groups. F. Cell viability was evaluated using CCK8 in the sAT and sAT + siHIF-1α groups. G. Apoptosis rate was determined by FACS in the sAT and sAT + siHIF-1α groups. H. Mitochondrial membrane potential was assessed using JC-1 staining in the sAT and sAT + siHIF-1α groups. × 200. I. ROS levels were measured by DHE staining in the sAT and sAT + siHIF-1α groups. × 200. J. sAT modulated the expression of apelin 13 partially through HIF-1α upregulation. The columns and error bars represent the means ± SDs (n = 3). $^{\#\#}P$ < 0.01 *vs* Con; $^{**}P$ < 0.01 *vs* model; $^{\&\&}P$ < 0.01 *vs* sAT treatment group.

MAPK/ATF4. Indeed, sAT exhibited inhibitory effects on P38 MAPK/ATF4. Further confirmatory experiments revealed that enhancing the upregulation of apelin expression by sAT can be achieved by inhibiting P38 MAPK with an inhibitor or siRNA knockdown of ATF4, intensifying the protective effects of sAT. Based on these results, we confirmed that sAT partially induced apelin expression by inhibiting P38 MAPK/ATF4.

5. Conclusion

In conclusion, this study demonstrated that sAT mitigated I/R-induced nerve cell injury by activating the apelin/AR-mediated pathway. Additionally, the research revealed that inhibition of P38 MAPK/ATF4 and activation of HIF-1α contributed to the effects of sAT on apelin/AR in the brain. These findings not only elucidate the potential mechanism and effective components of sAT but also suggest that the apelin/AR system may serve as a significant target for ischaemic events in the brain.

Funding

This work was supported by the National Science Foundation of China (No. 81903832), the Key Research and Development Plan of Shaanxi Province (No. 2022SF-182), the Fundamental Research Funds for the Central Universities (No. D5000210799), Shaanxi Provincial Traditional Chinese Medicine Administration "Double Chain Integration" Middle Youth Research and Innovation Team Project (No. 2022-SLRH-LJ-007), and Shanghai Science and Technology Innovation Action Plan (No. 22S21902600).

Supporting Information

Supporting information for this study is available upon re-

quest via email to the corresponding author.

Declaration of competing interest

These authors have no conflict of interest to declare.

References

1 Xu Y, Liu J, Zeng Y, et al. Traditional uses, phytochemistry, pharmacology, toxicity and quality control of medicinal genus *Aralia*: a review. *J Ethnopharmacol*. 2022;284(298):114671. https://doi.org/10.3389/fphar.2021.726528.

2 Clement JA, Clement ES . The medicinal chemistry of genus *Aralia*. *Curr Top Med Chem*. 2015;14(24):2783-801. https://doi.org/10.2174/1568026615666141208110021.

3 Weng Y, Yu L, Cui J, et al. Antihyperglycemic, hypolipidemic and antioxidant activities of total saponins extracted from *Aralia taibaiensis* in experimental type 2 diabetic rats. *J Ethnopharmacol*. 2014;152(3):553-560. https://doi.org/10.1016/j.jep.2014.02.001.

4 Xi M, Hai C, Tang H, et al. Antioxidant and antiglycation properties of total saponins extracted from traditional Chinese medicine used to treat diabetes mellitus. *Phytother Res*. 2008;22(2):228-237. https://doi.org/10.1002/ptr.2297.

5 Duan J, Cui J, Yang Z, et al. Neuroprotective effect of Apelin 13 on ischemic stroke by activating AMPK/GSK-3β/Nrf2 signaling. *J Neuroinflammation*. 2019;16(1):24. https://doi.org/10.1186/s12974-019-1406-7.

6 Chen D, Lee J, Gu X, et al. Intranasal delivery of apelin-13 is neuroprotective and promotes angiogenesis after ischemic stroke in mice. *ASN Neuro*. 2015;7(5):1759091415605114. https://doi.org/10.1177/1759091415605114.

7 Duan J, Cui J, Zheng H, et al. *Aralia taibaiensis* protects against I/R-induced brain cell injury through the Akt/SIRT1/FOXO3a pathway. *Oxid Med Cell Longev*. 2019;2019(284):7609765. https://doi.org/10.1155/2019/7609765.

8 Paul S, Candelario-Jalil E. Emerging neuroprotective strategies for the treatment of ischemic stroke: an overview of clinical and preclinical studies. *Exp Neurol*. 2021;335:113518. https://doi.org/10.1016/j.expneurol.2020.113518.

9 Manuel Y. Fibrinolytic and non-fibrinolytic roles of tissue-type plasminogen activator in the ischemic brain. *Neuroscience*. 2024;542:69-80. https://doi.org/10.1016/j.neuroscience.2023.08.011.

10 Tao YY, Ma JW, Feng. YZ, et al. Tissue-type plasminogen activator (tPA) homozygous Tyr471His mutation associates with thromboembolic disease. *MedComm*. 2023;4(5):e392-e392. https://doi.org/10.1002/mco2.392.

11 Zhou X, Chen H, Wang L, et al. Mitochondrial dynamics: a potential therapeutic target for ischemic stroke. *Front Aging Neurosci*. 2021;13:721428. https://doi.org/10.3389/fnagi.2021.721428.

12 Luo H, Gu X, Tong G, et al. Research progress of apelin in acute ischemic brain injury. *Am J Transl Res*. 2022;14(10):7260-7267.

13 Mughal A, O'Rourke ST. Vascular effects of apelin: mechanisms and therapeutic potential. *Pharmacol Ther*. 2018;190(2018):139-147. https://doi.org/10.1016/j.pharmthera.2018.05.013.

14 Hu J, Longmeng C, Dachao T, et al. Endogenous ligand of the APJ receptor apelin-13 inhibits cell apoptosis and oxidative stress of cardiomyocytes. *Cell Mol Biol*. 2023;69(11):207-212.

15 Razieh AZ, Hossein J, Saeed EM, et al. Effects of intracerebroventricular injection of apelin-13 on food intake in broiler chicks. *Vet Res forum*. 2023;14(2):105-108.

16 Zhang Y, Jiang WW, Sun WJ, et al. Neuroprotective roles of apelin-13 in neurological diseases. *Neurochem Res*. 2023;48(6):1648-1662. https://doi.org/10.1007/s11064-023-03869-0.

17 Duan J, Wei G, Guo C, et al. *Aralia taibaiensis* protects cardiac myocytes against high glucose-induced oxidative stress and apoptosis. *Am J Chin Med*. 2015;43(6):1159-1175. https://doi.org/10.1142/S0192415X15500664.

18 Vakili A, Zahedi khorasani M. Post-ischemic treatment of pentoxifylline reduces cortical not striatal infarct volume in transient model of focal cerebral ischemia in rat. *Brain Res*. 2007;1144(2007):186-191. https://doi.org/10.1016/j.brainres.2007.01.096.

19 Park SH, Lee AR, Choi K, et al. TOMM20 as a potential therapeutic target of colorectal cancer. *BMB Rep*. 2019;52(12):712-717. https://doi.org/10.5483/BMBRep.2019.52.12.249.

20 Biswas T, Dwivedi UN. Plant triterpenoid saponins: biosynthesis, *in vitro* production, and pharmacological relevance. *Protoplasma*. 2019;256(6):1463-1486. https://doi.org/10.1007/s00709-019-01411-0.

21 Fan C, Wang JX, Xiong ZE, et al. Saponins from *Panax japonicus* improve neuronal mitochondrial injury of aging rats. *Pharm Biol*. 2023;61(1):1401-1412. https://doi.org/10.1080/13880209.2023.2244532.

22 Sun A, Xu X, Lin J, et al. Neuroprotection by saponins. *Phytother Res*. 2015;29(2):187-200. https://doi.org/10.1002/ptr.5246.

23 Duan J, Yin Y, Wei G, et al. Chikusetsu saponin IVa confers cardioprotection *via* SIRT1/ERK1/2 and Homer1a pathway. *Sci Rep*. 2015;5(1):18123. https://doi.org/10.1038/srep18123.

24 Yan J, Duan J, Wu X, et al. Total saponins from *Aralia taibaiensis* protect against myocardial ischemia/reperfusion injury through AMPK pathway. *Int J Mol Med*. 2015;36(6):1538-1546. https://doi.org/10.3892/ijmm.2015.2391.

25 Xu W, Li T, Gao L, et al. Apelin-13/APJ system attenuates early brain injury *via* suppression of endoplasmic reticulum stress-associated TXNIP/NLRP3 inflammasome activation and oxidative stress in a AMPK-dependent manner after subarachnoid hemorrhage in rats. *J Neuroinflammation*. 2019;16(1):247. https://doi.org/10.1186/s12974-019-1620-3.

26 Shao ZQ, Dou SS, Zhu JG, et al. Apelin-13 inhibits apoptosis and excessive autophagy in cerebral ischemia/reperfusion injury. *Neural Regen Res*. 2021;16(6):1044-1051. https://doi.org/10.4103/1673-5374.300725.

27 Stefania DA, Elena M, Federico DF, et al. Sirt1 activity in the brain: simultaneous effects on energy homeostasis and reproduction. *Int J Environ Res Public Health*. 2021;18(3):1243-1243. https://doi.org/10.3390/IJERPH18031243.

28 Meng XF, Tan J, Li MM, et al. Sirt1: role under the condition of ischemia/hypoxia. *Cell Mol Neurobiol*. 2017;37(1):17-28. https://doi.org/10.1007/s10571-016-0355-2.

29 Olmos Y, Sánchez-Gómez FJ, Wild B, et al. SirT1 regulation of antioxidant genes is dependent on the formation of a FoxO3a/PGC-1α complex. *Antioxid Redox Signal*. 2013;19(13):1507-1521. https://doi.org/10.1089/ars.2012.4713.

30 Halling JF, Pilegaard H. PGC-1α-mediated regulation of mitochondrial function and physiological implications. *Appl Physiol Nutr Metab*. 2020;45(9):927-936. https://doi.org/10.1139/apnm-2020-0005.

31 Wu Y, Wang X, Zhou X, et al. Temporal expression of apelin/apelin receptor in ischemic stroke and its therapeutic potential. *Front Mol Neurosci*. 2017;10:1. https://doi.org/10.3389/fnmol.2017.00001.

32 Rastaldo R, Cappello S, Folino A, et al. Effect of apelin-apelin receptor system in postischaemic myocardial protection: a pharmacological postconditioning tool?. *Antioxid Redox Signal*. 2011;14(5):909-922. https://doi.org/10.1089/ars.2010.3355.

33 He L, Xu J, Chen L, et al. Apelin/APJ signaling in hypoxia-related diseases. *Clin Chim Acta*. 2015;451(Pt B):191-198. https://doi.org/10.1016/j.cca.2015.09.029.

34 Liang Z, Wu G, Fan C, et al. The emerging role of signal transducer and activator of transcription 3 in cerebral ischemic and hemorrhagic stroke. *Prog Neurobiol*. 2016;137:1-16. https://doi.org/10.1016/j.pneurobio.2015.11.001.

35 Morimoto N, Oida Y, Shimazawa M, et al. Involvement of endoplasmic reticulum stress after middle cerebral artery occlusion in mice. *Neuroscience*. 2007;147(4):957-967. https://doi.org/10.1016/j.neuroscience.2007.04.017.

36 Iwanaga Y, Kihara Y, Takenaka H, et al. Down-regulation of cardiac apelin system in hypertrophied and failing hearts: possible role of angiotensin II-angiotensin type 1 receptor system. *J Mol Cell Cardiol*. 2006;41(5):798-806. https://doi.org/10.1016/j.yjmcc.2006.07.004.

37 Jeong K, Oh Y, Kim SJ, et al. Apelin is transcriptionally regulated by ER stress-induced ATF4 expression *via* a p38 MAPK-dependent pathway. *Apoptosis*. 2014;19(9):1399-1410. https://doi.org/10.1007/s10495-014-1013-0.

38 Wang H, Qi J, Li L, et al. Inhibitory effects of chikusetsusaponin IVa on lipopolysaccharide-induced pro-inflammatory responses in THP-1 cells. *Int J Immunopathol Pharmacol*. 2015;28(3):308-317. https://doi.org/10.1177/0394632015589519.